Scientific Research Publishing

Advances in Materials Physics and Chemistry, 2017, 7, 364-374
http://www.scirp.org/journal/ampc
ISSN Online: 2162-5328
ISSN Print: 2162-531X

A High Power Carbon/LiM_xO_y Hybrid Cathode for Non-Aqueous Li-O_2 Battery

Ming Song*, Jing Peng, Xiang Yu

College of Chemistry and Chemical Engineering, Xuzhou University of Technology, Xuzhou, China
Email: *mings@xzit.edu.cn

How to cite this paper: Song, M., Peng, J. and Yu, X. (2017) A High Power Carbon/LiM_xO_y Hybrid Cathode for Non-Aqueous Li-O_2 Battery. *Advances in Materials Physics and Chemistry*, **7**, 364-374.
https://doi.org/10.4236/ampc.2017.710029

Received: September 29, 2017
Accepted: October 27, 2017
Published: October 30, 2017

Abstract

Among all the issues that restrict the application of Li-air battery, poor power performances of O_2 cathode comes first. In this paper, we establish carbon (Super P)/LiM_xO_y ($LiMn_2O_4$/$LiFePO_4$/$LiNi_{1/3}Co_{1/3}Mn_{1/3}O_2$) hybrid cathode to promote the power output of conventional carbon cathode through continuous Li^+-insertion reaction of LiM_xO_y and Li^+ transportation in bulk LiM_xO_y during the discharging process. Weight and volume specific power performances of the hybrid cathode are much higher than those of traditional Super P carbon cathode. The mechanism of improving power performance of O_2 cathode has also been discussed through electrochemical impedance spectroscopy and cyclic voltammetry method in this paper.

Keywords

Power Performance, Li-O_2 Battery, Hybrid Cathode

1. Introduction

The non-aqueousLi-air (Li-O_2) batteries have attracted great attention owing to the highest theoretical specific energy (3505 $Wh{\cdot}kg^{-1}$) among various energy storage systems [1] [2] [3]. However, the development of Li-O_2 batteries is largely lagged by low round-trip efficiency [4] [5] [6] [7] (caused by decomposition of non-aqueous electrolyte and carbon based oxygen electrode), short cycle life [8] [9] [10] (caused by non-recovery of reaction surface/interface), and poor power capability [11] [12] [13] (caused by low kinetics of electron, Li_+ and O_2 transport) during oxygen reduction reaction (ORR) and oxygen evolution reaction (OER). The low round-trip efficiency and short cycle life issues mentioned above have attracted great attentions in recent years [14] [15] [16]. More importantly, the power ability of the non-aqueous Li-O_2 battery (no advantage com-

pare to Li-ion battery) [17], should be improved as well since high power output are required if it is expected to be developed for portable device and electric transportation.

For non-aqueous Li-O_2 battery, sluggish ORR process of the O_2 cathode, during which O_2 is, principally, reduced to produce Li_2O_2 on cathode surface, gives rise to the poor power output. Insolubility and low ionic/electronic conductivity of Li_2O_2 [18] [19] [20] mean it is difficult to transport electron and Li^+ to the reaction interface through bulk Li_2O_2. Low O_2 solubility and transportation in electrolyte mean it is hard to supply sufficient O_2, especially under high current density [11] [21] [22] [23].

To improve the poor power ability of O_2 cathode mentioned above, researchers have focused on how to promote the ORR catalysis, oxygen and ionic/electronic transport. Although the catalysis mechanism is still in dispute, ORR catalysts have been found to play a key role in improving the power ability of the O_2 cathode [24] [25] [26]. In addition, continuous passage construction for gaseous O_2 through cathode design could provide a specific power more than 1600 $W{\cdot}kg^{-1}$ [21] and faster Li^+ transport in Li_2O_2 could also promote the power ability of O_2 cathode [27]. However, awkward problems (e.g., catalysts are easily deactivated and O_2/electrolyte/Li_2O_2 reaction interfaces are limited when Li_2O_2 deposit on the cathode surface) still exist and need to be tackled.

In this paper, a novel strategy to readily enhance the poor power ability of the non-aqueous Li-O_2 battery has been demonstrated. Super P (Superconductive carbon)/LiM_xO_y ($LiMn_2O_4$/$LiFePO_4$/$LiNi_{1/3}Co_{1/3}Mn_{1/3}O_2$) hybrid cathode (SLHC) is established to improve the power performance of conventional Super P cathode (SC) through continuous Li^+-insertion reaction of LiM_xO_y to provide additional cathodic reactions and continuous Li^+ transportation of LiM_xO_y to extended additional reaction interfaces. This method may provide a new direction for promoting the power performances for the non-aqueous Li-O_2 batteries.

2. Experimental

Super P cathode (SC) and Super P /LiM_xO_y hybrid cathode (SLHC) used in this paper were prepared by coating a Super P carbon (70 wt.%)/PTFE (30 wt.%) or Super P carbon (20 wt.%)/$LiMn_2O_4$ (50/3 wt.%)/$LiFePO_4$ (50/3 wt.%)/$LiNi_{1/3}Co_{1/3}Mn_{1/3}O_2$ (50/3 wt.%))/PTFE (30 wt.%) (Shenzhen Kejingstar, Ltd.), respectively, slurry onto a Ni foam304 SS mesh (Shenzhen Kejingstar, Ltd.) with a diameter of 1.4 cm and the electrolytes were prepared by mixing lithium trifluoromethane sulfonimide (LiTFSI) in tetraglyme (TEGDME) (Aladdin-Reagent, Inc.) with the molar ratio between LiTFSI and TEGDME is 1:5 (~0.89 M) in a glove box (MikrounaChina Co., Ltd.) filled with argon ([H_2O] < 0.1 ppm). More details about the cathodes and electrolytes preparations can be found elsewhere [28].

The Li-O_2 battery configuration used in this paper has been described elsewhere [29], including a lithium foil (1.6 cm in diameter), one pieces of Whatman

glass microfibre filters separator (1.9 cm in diameter), and a SC or SLHC cathode (1.4 cm in diameter). The cell was assembled in a glove box with water contents of <0.1 ppm, and about 300 μl prepared electrolyte was added in each cell. After standing for at least 24 h at room temperature, cells were discharged and charged under O_2 with a 1.1 atm pressure using a New are Battery Testing System (CT-3008, Shenzhen Newear Co., Ltd.).

Electrochemical impedance spectroscopy (EIS) was measured by a CHI660E (CH Instruments, Inc.) and the spectra were obtained in the frequency range from 1 MHz to 100 mHz with an AC amplitude of 5 mV at 0% deep of discharge (DOD).

Cyclic voltammetry (CV) was also measured by a CHI660E with the scan speed of 10 $mV \cdot s^{-1}$ from the open circuit potential (OCP) to 2 V (vs. Li^+/Li) and then, 4.5 V (vs. Li^+/Li).

3. Results and Discussion

3.1. Power Performances of SLHC and SC

Galvanostatic discharge method was used to reveal the power performance of SLHC and SC. The second discharge profiles of the SLHC and SC at a current density of 0.1 $mA \cdot cm^{-2}$ (Figure 1) are illustrated since LiM_xO_y need "activation" during the first charging process ($LiM_xO_y - zLi^+ - ze^- \rightarrow Li_{1-z}M_xO_y$). The second discharge process of the SLHC consists of two kinds cathodic reactions. The first one is conventional Li^+-insertion reaction ($Li_{1-z}M_xO_y + zLi^+ + ze^- \rightarrow LiM_xO_y$) at different voltage (~3.8 V for $Li_{1-z}Mn_2O_4$, ~3.6 V for $Li_{1-z}Ni_{1/3}Co_{1/3}Mn_{1/3}O_2$ and ~3.4V for $Li_{1-z}FePO_4$) and the second one is ORR ($2Li^+ + O_2 + 2e^- \rightarrow Li_2O_2$) at about 2.5 - 2.6 V. Obviously, under 0.1 $mA \cdot cm^{-2}$, Li^+-insertion reaction dominates the initial parts (ORR dominates the rest) of discharge processes of SLHC, which are different from those of SC. Since

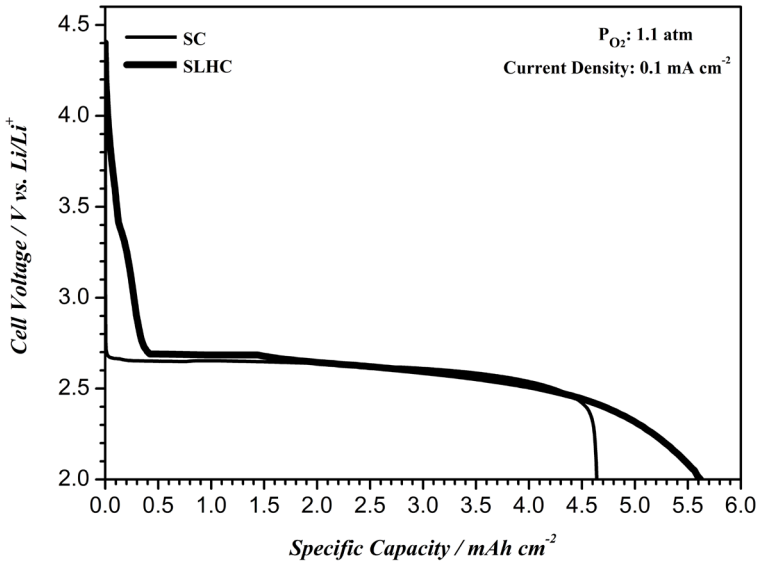

Figure 1. Discharge profiles of the SLHC and SC at 0.1 $mA \cdot cm^{-2}$.

most parts of discharge processes of SLHC are ORR, the specific capacities of SLHC are a little larger than those of SC. In addition, under 0.1 mA·cm^{-2}, ORR voltage plateaus are about 2.7 V vs. Li/Li$^+$ (2.96 V in theory), which reveals the a dynamic characteristic of ORR.

As for the power performances (P = V*I) of SLHC and SC, it is vital important to keep high voltages output at large discharge currents. **Figure 2** compares the 600 s polarization curves for both the SLHC and SC at three current densities. During the short test process, Li$^+$-insertion reaction are dominative for SLHC and while, ORR still dominate most parts of discharge processes of SC. Furthermore, due to the collaborative advantage of specific capacities and Li$^+$-insertion potentials for $LiMn_2O_4$, $LiFePO_4$ and $LiNi_{1/3}Co_{1/3}Mn_{1/3}O_2$, the polarization of the SLHC is much smaller than that of SC at all current densities. It is worth noting that, under high current density, the average voltage difference of SLHC and SC is larger in shorter test process. For example, when the current density rises from 0.1 to 0.3 mA·cm^{-2}, the average voltage (E_{50s}) differences of SLHC and SC increase from about 0.7 to 1.4 V vs. Li/Li$^+$ This excellent depolarization effect of SLHC should provide a substantially enhanced power output. As is shown in **Figure 3**, at low current density (0.1 mA·cm^{-2}), the weight specific power (P_w, **Figure 3(a)**) and volume specific power (Pv, **Figure 3(b)**) of SLHC in 50 s is 13.2 W·kg$^{-1}{}_{cathode}$ and 2685 W·m$^{-3}{}_{cathode}$, respectively, which is a little higher than that of SC (11.5 W·kg$^{-1}{}_{cathode}$ and 2129 W·m$^{-3}{}_{cathode}$). However, with the increase of current density from 0.1 mA·cm^{-2} to 0.3 mA·cm^{-2}, obviously, the P_w and P_v differences in 50 s between SLHC and SC become larger. At 0.3 mA·cm^{-2}, P_w and P_v of SLHC are 36.9 W·kg$^{-1}{}_{cathode}$ and 7507 W·m$^{-3}{}_{cathode}$, respectively, which is much higher than that of SC (25.4 W·kg$^{-1}{}_{cathode}$ and 4712 W·m$^{-3}{}_{cathode}$). In addition, similar results can be observed in 600 s as shown in **Figure 3**. More

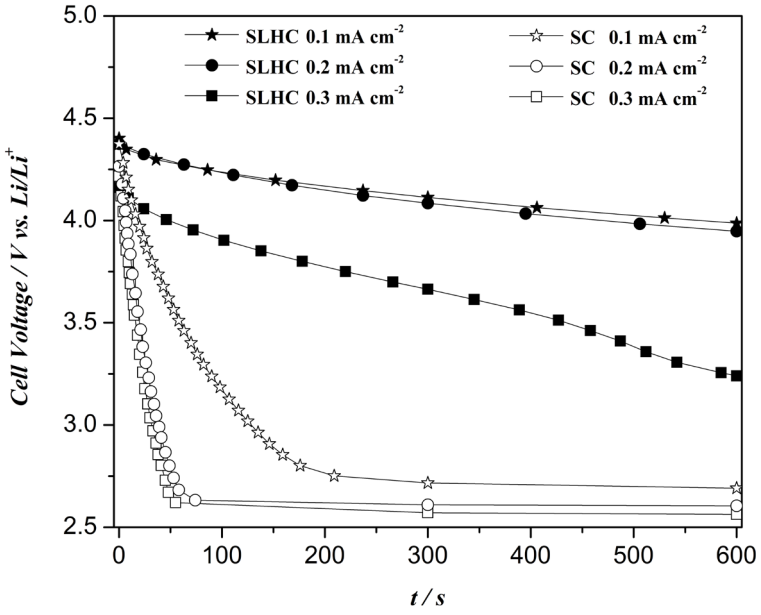

Figure 2. Galvanostatic polarization curves of the SLHC and SC.

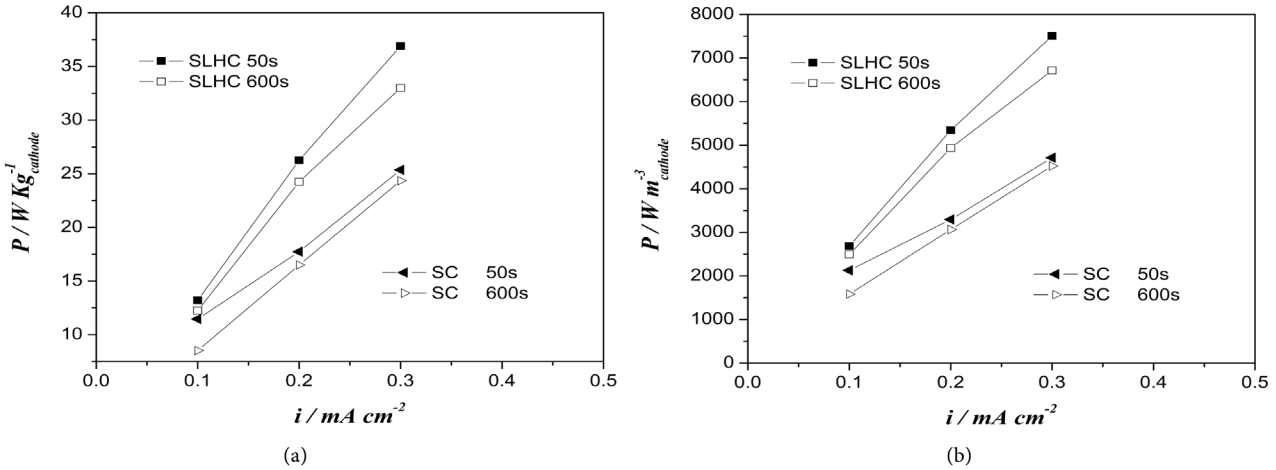

Figure 3. (a) Weight and (b) volume specific power performances of the SLHC and SC (based on total weight and volume of the electrode, SLHC-50.1 mg/0.246 cm^3, SC-47.6 mg/0.261 cm^3).

importantly, it can be speculated that at much higher current density, these advantages in power performances of SLHC should be more remarkable.

3.2. High Power Output Mechanism of SLHC

Cyclic voltammetry is carried out to study the electrochemical process of SLHC since it is a useful technique for discerning kinetics and mechanisms of electrochemical reactions. The potential for full-range cyclic voltammograms (CVs) is first swept from OCP of around 2.9 V to 2.0 V vs. Li/Li^+, and then it is reversed to anodic direction (**Figure 4**). During the first cathodic scan process, no obvious cathodic peaks (P_c) are observed for both SLHC and SC, which indicates a poor kinetic characteristic of ORR. When the scan reverses to anodic direction, the current of SLHC responds more strongly than that of SC, which may attribute to the "activation" of LiM_xO_y ($LiM_xO_y - zLi^+ - ze^- \rightarrow Li_{1-z}M_xO_y$) mentioned above. A gentle anodic peak (P_a) around 3.5 V vs. Li/Li^+ is observed in **Figure 4** reflects the OER process ($Li_2O_2 \rightarrow 2Li^+ + 2e^- + O_2$) and no sharp P_a exists because of the solution-like delithiation and two-phase oxidation processes [30]. It is worth to note that, during the second cathodic scan, the cathodic current below 4.0 V vs. Li/Li^+ may come from the Li^+-insertion reaction at different voltage (~3.8 V for $Li_{1-z}Mn_2O_4$, ~3.6 V for $Li_{1-z}Ni_{1/3}Co_{1/3}Mn_{1/3}O_2$ and ~3.4 V for $Li_{1-z}FePO_4$). Furthermore, addition of LiM_xO_y in SLHC also benefit ORR process since an obvious P_c around 2.5 V is observed for SLHC, which is different from that of SC (**Figure 4**).

The discharging processes of SLHC and SC are schematically displayed in **Figure 5**. For SC, Li_2O_2 (insolubility and low ionic/electronic conductivity) covers on the outer space of C/electrolyte interface during the discharging process, which gives rise to the poor kinetic characteristic of ORR. However, the addition of LiM_xO_y in SLHC plays two vital roles. First, Li^+-insertion reaction of LiM_xO_y during the discharging process could benefit the power output of SLHC (**Figure 3**). Second, Li^+ could diffuse through bulk LiM_xO_y to the inner reaction interface,

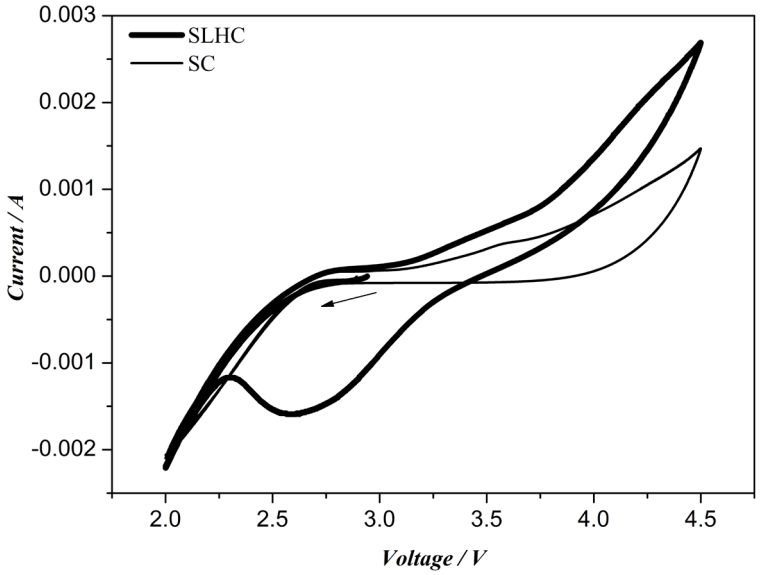

Figure 4. Cyclic voltammograms for SLHC and SC in the voltage range between 2 and 4.5 V. The potential was swept at a scan rate of 10 mV/s.

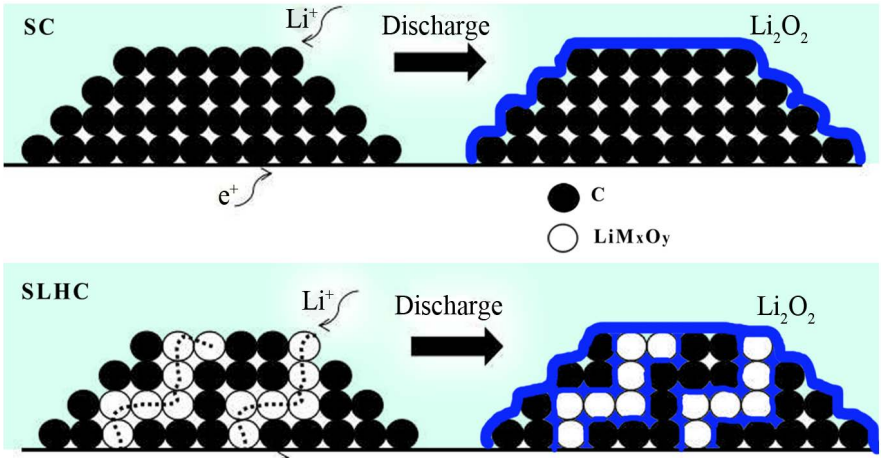

Figure 5. Schematic representation of the discharging process of SLHC and SC.

which benefit the ORR process (**Figure 4**) and electrochemical performance (**Figure 1**) of SLHC.

EIS is further introduced to the study of the kinetic properties of SLHC and SCat 0% DOD (**Figure 6**). Laoire *et al.* [31] interpreted the impedance spectra of Li-O_2 batteries and proposed the equivalent circuit (Rs (C (RpW)), where C is the capacitive contributions of the two electrodes, R_s is the electronic resistance of the electrodes and their contacts to the current collectors, and electrolyte resistance, R_p is the charge transfer resistance at the two electrodes, W is the linear Warburg element that may be attributed to the diffusion of the electroactive species to the electrode. As shown in **Figure 6**, the charge-transfer resistance R_p of SLHC is a little larger than that of SC, probably because of the lower electronic conductivity of LiM_xO_y compared with C. At very low frequencies, there is a re-

gion in which a typical Warburg behaviour, related to the diffusion of lithium ions in the cathode active material, is seen. By using the model proposed by Ho *et al.* [32], the diffusion coefficient for SLHC and SC are calculated by using Equation (1).

$$D_{Li} = 1/2\left[\left(V_M/SFA\right)\left(\delta E/\delta x\right)\right]^2 \quad (1)$$

where V_M is the molar volume (SLHC-10.23 $cm^3 \cdot mol^{-1}$, SC-5.28 $cm^3 \cdot mol^{-1}$), S is the contact area between electrolyte and sample (1.54 cm^2), F is the Faraday constant (96,486 $C \cdot mol^{-1}$), A is the plot slope of imaginary resistance (Zim.) vs. inverse square root of angular frequency $\left(1/\sqrt{2\pi f}\right)$, which can be obtained from

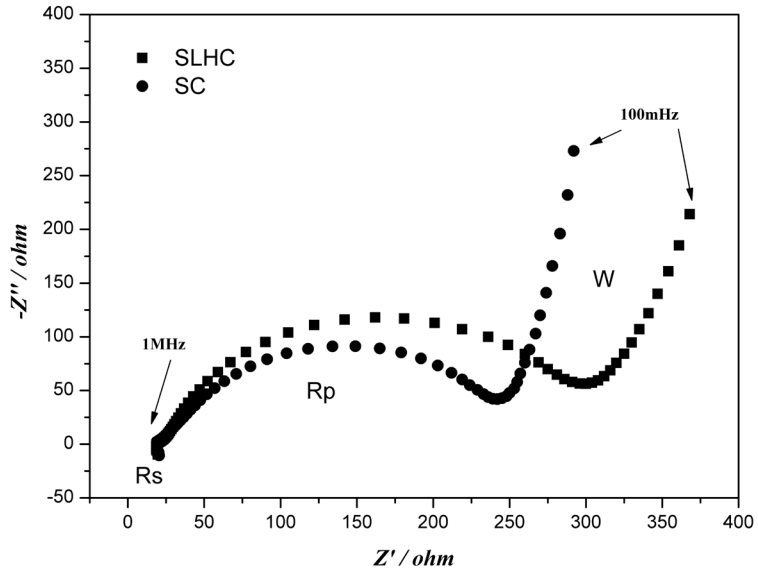

Figure 6. Nyquist plots of SLHC and SC.

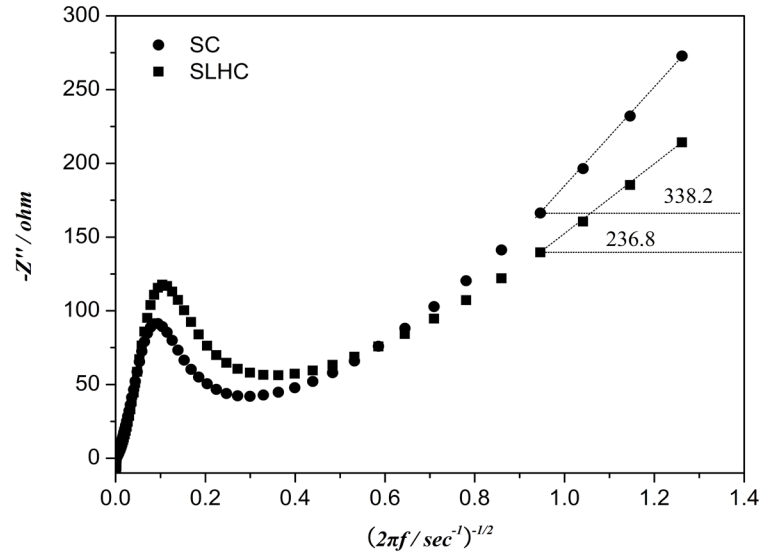

Figure 7. The plot of the imaginary resistance as a function of the inverse square root of angular speed for SLHC and SC. Data obtained from impedance spectroscopy.

the Warburg impedance, and $\delta E/\delta x$ is the slope of galvanostatic charge-discharge curves (SLHC, −1.284, SC, −0.424).

Figure 7 shows the plot of the imaginary resistance determined by impedance spectroscopy as a function of the inverse square root of the angular frequency for SLHC and SC. Linear behaviors of SLHC and SC are observed for frequency values ranging from 100 m·Hz to 178 m·Hz with a slope of 236.8 $\Omega \cdot s^{-1}$ and 338.2 $\Omega \cdot s^{-1}$, respectively. The diffusion coefficients of lithium for SLHC (5.43×10^{-15} $cm^2 \cdot s^{-1}$) and SC (2.33×10^{-15} $cm^2 \cdot s^{-1}$) obtained by substitution of the curve slopes in Equation (1). This result of D_{Li} is fairly in agreement with that of CV (Figure 4) and galvanostatic charging (Figure 1).

4. Conclusions

The power output ability of cathode for non-aqueous Li-O_2 battery has been improved by simply adding LiM_xO_y into the conventional Super P carbon cathode. LiM_xO_y benefits the power output of cathode through providing additional Li^+-insertion reaction and Li^+ diffusion in bulk LiM_xO_y. At 0.3 $mA \cdot cm^{-2}$, Weight and volume specific power performances of the SLHC are 36.9 $W \cdot kg^{-1}_{cathode}$ and 7507 $W \cdot m^{-3}_{cathode}$, respectively, which is much higher than those of SC (25.4 $W \cdot kg^{-1}_{cathode}$ and 4712 $W \cdot m^{-3}_{cathode}$).

CVs of SLHC reveal that Li^+-insertion reaction occurs at different voltages (~3.8 V for $Li_{1-z}Mn_2O_4$, ~3.6 V for $Li_{1-z}Ni_{1/3}Co_{1/3}Mn_{1/3}O_2$ and ~3.4 V for $Li_{1-z}FePO_4$) and improved ORR kinetics has been observed during the second discharging process. Furthermore, Li^+ diffusion in SLHC is faster than in SC according to the EIS results.

These results may provide a new direction for promoting the power performances of non-aqueous Li-O_2 batteries and this method may be applied in other metal-O_2 batteries.

Acknowledgements

This study was financially supported by the Natural Science Foundation of Jiangsu Province, China (Grant No. BK20171169), the Natural Science Foundation of the Jiangsu Higher Education Institutions of China (Grant No. 16KJB150037), the Research Project of Xuzhou University of Technology, China (Grant No. XKY2015307).

References

[1] An, B., Ru, Q., Hu, S., Song, X. and Li, J. (2014) Facile Synthesis and Electrochemical Performance of Co_2SnO_4/Co_3O_4 Nanocomposite for Lithium-Ion Batteries. *Materials Research Bulletin*, **60**, 640-647. https://doi.org/10.1016/j.materresbull.2014.09.020

[2] Luntz, A.C. and McCloskey, B.D. (2014) Nonaqueous Li-Air Batteries: A Status Report. *Chemical Reviews*, **114**, 11721-11750. https://doi.org/10.1021/cr500054y

[3] Bruce, P.G., Freunberger, S.A., Hardwick, L.J. and Tarascon, J.M. (2012) Li-O_2 and Li-S batteries with High Energy Storage. *Nature Materials*, **11**, 19-29.

https://doi.org/10.1038/nmat3191

[4] McCloskey, B.D., Speidel, A., Scheffler, R., Miller, D.C., Viswanathan, V., Hummelshøj, J.S., Nørskov, J.K. and Luntz, A.C. (2012) Twin Problems of Interfacial Carbonate Formation in Nonaqueous Li-O_2 Batteries. *The Journal of Physical Chemistry Letters*, **3**, 997-1001. https://doi.org/10.1021/jz300243r

[5] Thotiyl, M.M.O., Freunberger, S.A., Peng, Z. and Bruce, P.G. (2013) The Carbon Electrode in Nonaqueous Li-O_2 Cells. *Journal of the American Chemical Society*, **135**, 494-500. https://doi.org/10.1021/ja310258x

[6] S.A. Freunberger, Y. Chen, Z. Peng, J.M. Griffin, L.J. Hardwick, F. Bardé, P. Novák and Bruce, P.G. (2011) Reactions in the Rechargeable Lithium-O_2 Battery with Alkyl Carbonate Electrolytes. *Journal of the American Chemical Society*, **133**, 8040-8047. https://doi.org/10.1021/ja2021747

[7] Bryantsev, V.S. and Faglioni, F. (2012) Predicting Autoxidation Stability of Ether- and Amide-Based Electrolyte Solvents for Li-Air Batteries. *Journal of the American Chemical Society*, **116**, 7128-7138. https://doi.org/10.1021/jp301537w

[8] Li, F., Zhang, T., Yamada, Y., Yamada, A. and Zhou, H.S (2013) Enhanced Cycling Performance of Li-O_2 Batteries by the Optimized Electrolyte Concentration of LiTFSA in Glymes. *Advanced Energy Materials*, **3**, 532-538. https://doi.org/10.1002/aenm.201200776

[9] Zhang, D., Fu, Z., Wei, Z., Huang, T. and Yu, A. (2010) Polarization of Oxygen Electrode in Rechargeable Lithium Oxygen Batteries. *Journal of the Electrochemical Society*, **157**, A362-A365. https://doi.org/10.1149/1.3298450

[10] Viswanathan, V., Thygesen, K.S., Hummelshøj, J.S., Nørskov, J.K. and Girishkumar, G. (2011) Electrical Conductivity in Li_2O_2 and Its Role in Determining Capacity Limitations in Non-Aqueous Li-O_2 Batteries. *The Journal of Chemical Physics*, **135**, 214704(1)-214704(10).

[11] Zhu, D., Zhang, L., Song, M., Wang, X., Mi, R., Liu, H., Mei, J., Lau, L. and Chen, Y. (2013) Intermittent Operation of the Aprotic Li-O_2 Battery: The Mass Recovery Process upon Discharge Interval. *Journal of Solid State Electrochemistry*, **17**, 2539-2544. https://doi.org/10.1007/s10008-013-2116-1

[12] Monaco, S., Soavi, F. and Mastragostino, M. (2013) Role of Oxygen Mass Transport in Rechargeable Li/O_2 Batteries Operating with Ionic Liquids. *The Journal of Physical Chemistry Letters*, **4**, 1379-1382. https://doi.org/10.1021/jz4006256

[13] Albertus, P., Girishkumar, G., McCloskey, B.D., Carrera, R.S.S., Kozinsky, B., Christensen, J. and Luntz, A.C. (2011) Identifying Capacity Limitations in the Li/Oxygen Battery Using Experiments and Modeling. *Journal of the Electrochemical Society*, **158**, A343-A351. https://doi.org/10.1149/1.3527055

[14] Song, S., Xu, W., Zheng, J., Luo, L., Engelhard, M.H., Bowden, M.E., Liu, B., Wang, C.M. and Zhang, J.G. (2017) Complete Decomposition of Li_2CO_3 in Li-O_2 Batteries Using Ir/B_4C as Noncarbon-Based Oxygen Electrode. *Nano Letters*, **17**, 1417-1424. https://doi.org/10.1021/acs.nanolett.6b04371

[15] Hu, X., Wang, J., Li, Z., Wang, J., Gregory, D.H. and Chen, J. (2017) MCNTs@ MnO_2 Nanocomposite Cathode Integrated with Soluble O_2-Carrier Co-Salen in Electrolyte for High-Performance Li-Air Batteries. *Nano Letters*, **17**, 2073-2078. https://doi.org/10.1021/acs.nanolett.7b00203

[16] Liu, G., Zhang, L., Wang, S., Ding, L.X. and Wang, H. (2017) Hierarchical $NiCo_2O_4$ Nanosheets on Carbon Nanofiber Films for High Energy Density and Long-Life Li-O_2 Batteries. *Journal of Materials Chemistry A*, **5**, 14530-14536. https://doi.org/10.1039/C7TA03703A

[17] Oh, S.H. and Nazar, L.F. (2012) Oxide Catalysts for Rechargeable High-Capacity Li-O_2 Batteries. *Advanced Energy Materials*, **2**, 903-910. https://doi.org/10.1002/aenm.201200018

[18] Kang, J., Jung, Y.S., Wei, S.H. and Dillon, A.C. (2012) Implications of the Formation of Small Polarons in Li_2O_2 for Li-Air Batteries. *Physical Review B*, **85**, 035210(1)-035210(5).

[19] Hummelshøj, J.S., Blomqvist, J., Datta, S., Vegge, T., Rossmeisl, J., Thygesen, K.S., Luntz, A.C., Jacobsen, K.W. and Nørskov, J.K. (2010) Communications: Elementary Oxygen Electrode Reactions in the Aprotic Li-Air Battery. *The Journal of Chemical Physics*, **132**, 071101(1)-071101(7).

[20] Zhong, L., Mitchell, R.R., Liu, Y., Gallant, B.M., Thompson, C.V., Huang, J.Y., Mao, S.X. and Shao-Horn, Y. (2013) In Situ Transmission Electron Microscopy Observations of Electrochemical Oxidation of Li_2O_2. *Nano Letters*, **13**, 2209-2214. https://doi.org/10.1021/nl400731w

[21] Zhang, T. and Zhou, H.S. (2012) From Li-O_2 to Li-Air Batteries: Carbon Nanotubes/Ionic Liquid Gels with a Tricontinuous Passage of Electrons, Ions, and Oxygen. *Angewandte Chemie International Edition*, **51**, 11062-11067. https://doi.org/10.1002/anie.201204983

[22] Cui, Y., Wen, Z., Liang, X., Lu, Y., Jin, Y., Wu, M. and Wu, X. (2012) A Tubular Polypyrrole Based Air Electrode with Improved O_2 Diffusivity for Li-O_2 Batteries, *Energy & Environmental Science*, **5**, 7893-7897. https://doi.org/10.1039/c2ee21638h

[23] Monaco, S., Soavi, F. and Mastragostino, M. (2013) Role of Oxygen Mass Transport in Rechargeable Li/O_2 Batteries Operating with Ionic Liquids. *The Journal of Physical Chemistry Letters*, **4**, 1379-1382. https://doi.org/10.1021/jz4006256

[24] Zhang, J., Wang, L., Xu, L., Ge, X., Zhao, X., Lai, M., Liu, Z. and Chen, W. (2015) Porous Cobalt-Manganese Oxide Nanocubes Derived from Metal Organic Frameworks as a Cathode Catalyst for Rechargeable Li-O_2 Batteries. *Nanoscale*, **7**, 720-726. https://doi.org/10.1039/C4NR05865H

[25] Zhang, P., Sun, D., He, M., Lang, J., Xu, S. and Yan, X. (2015) Synthesis of Porous δ-MnO_2 Submicron Tubes as Highly Efficient Electrocatalyst for Rechargeable Li-O_2 Batteries. *ChemSusChem*, **8**, 1972-1979. https://doi.org/10.1002/cssc.201500306

[26] Saito, M., Kosaka, S., Fujinami, T., Tachikawa, Y., Shiroishi, H., Streich, D., Berg. E.J., Novák, P. and Seki, S. (2017) A New Concept of an Air-Electrode Catalyst for Li_2O_2 Decomposition Using MnO_2 Nanosheets on Rechargeable Li-O_2 Batteries. *Electrochimica Acta*, **252**, 192-199. https://doi.org/10.1016/j.electacta.2017.08.183

[27] Lu, Y.C., Kwabi, D.G., Yao, K., Harding, J.R., Zhou, J., Zuin, L. and Shao-Horn, Y. (2011) The Discharge Rate Capability of Rechargeable Li-O_2 Batteries. *Energy & Environmental Science*, **4**, 2999-3007. https://doi.org/10.1039/c1ee01500a

[28] Song, M., Zhu, D., Zhang, L., Wang, X., Mi, R., Liu, H., Mei, J., Lau, L. and Chen, Y. (2014) Temperature Characteristics of Nonaqueous Li-O_2 Batteries. *Journal of Solid State Electrochemistry*, **18**, 739-745. https://doi.org/10.1007/s10008-013-2310-1

[29] Song, M., Zhu, D., Zhang, L., Wang, X., Huang, L., Shi, Q., Mi, R., Liu, H., Mei, J., Lau, L. and Chen, Y. (2013) Temperature Dependence of Charging Characteristic of C-Free Li_2O_2 Cathode in Li-O_2 Battery. *Journal of Solid State Electrochemistry*, **17**, 2061-2069. https://doi.org/10.1007/s10008-013-2067-6

[30] Gallant, B.M., Kwabi, D.G., Mitchell, R.R., Zhou, J., Thompson, C.V. and Shao-Horn, Y. (2013) Influence of Li_2O_2 Morphology on Oxygen Reduction and Evolution Kinetics in Li-O_2 Batteries. *Energy & Environmental Science*, **6**, 2518-2528.

https://doi.org/10.1039/c3ee40998h

[31] Laoire, C., Mukerjee, S., Plichta, E.J., Hendrickson, M.A. and Abraham, K.M. (2011) Rechargeable Lithium/TEGDME-$LiPF_6/O_2$ Battery. *Journal of the Electrochemical Society*, **158**, A302-A308. https://doi.org/10.1149/1.3531981

[32] Ho, C., Raistrick, I.D. and Huggins, R.A. (1980) Application of A-C Techniques to the Study of Lithium Diffusion in Tungsten Trioxide Thin Films. *Journal of the Electrochemical Society*, **127**, 343-350. https://doi.org/10.1149/1.2129668